

EARTHQUAKE SIMULATION AND RESPONSE OF WINE-BARREL STACKS

Gabriel Candia¹, Juan C. de la Llera², José L. Almazán²

1 M.Eng., Dept. of Struct. and Geotech. Engrg., Pontificia Universidad Católica de Chile. Santiago, Chile

2 Professor, Dept. of Struct. and Geotech. Engrg., Pontificia Universidad Católica de Chile. Santiago, Chile,

Email: jcllera@ing.puc.cl

ABSTRACT :

An analytical formulation was developed to simulate the earthquake behavior of wine barrel stacks. The model is cast using the fundamental steps of kinematics, action-deformation, and equilibrium of structural analysis. It assumes that interacting bodies are rigid and that the interaction forces between the bodies are properly represented by the use of nonlinear contact elements. Based on this theoretical model, it was possible to reproduce the overall behavior of the stack if appropriate contact element parameters are used. Contact elements are required to monitor the forces that are developed at the rack-ground and rack-barrel interfaces. It has been found that the maximum amplification of the normal stress on a body when the barrel stack is subjected to ground motions is about 3 times larger than the maximum stress due to self-weight. Furthermore, the properties of the physical contact elements were calibrated experimentally. Results of benchmark cases shows that the theoretical model is capable of representing the true collapse mechanism of the different stacks.

KEYWORDS: Wine barrel stacks, collapse modes, contact elements, tuned masses

1. INTRODUCTION

The earthquake behavior of wine barrel stacks was first studied experimentally by Marrow [1]. The global objectives of his research were to expand knowledge on the dynamic behavior of these systems, develop strategies to reduce the seismic risk of the stacks and the economic loss and impact in the wine industry in future earthquakes. Based on the experimental response of wine barrel stacks in shaking table experiments, diverse and complex modes of collapse were identified, such as sliding or rocking of the entire stack or part of the stack, and upthrow (ejection) of the barrels in the upper levels. Destructive tests were performed to determine the ultimate strength and ductility of barrel stacks, and the maximum height from which barrels could fall without breaking. As a result, low cost devices were developed oriented to enhance the earthquake performance of wine barrel stacks and prevent two of the most destructive modes of collapse: the top barrel ejection, and the rack walking and sliding. These protection devices are simple and are introduced to the standard rack without interfering with the production process.

In spite of the thorough experimental work accomplished, analytical results on the dynamic response of wine barrel stacks are few. The analytical formulation of this problem can be conveniently cast in terms of nonlinear rigid-body dynamics. The dynamic behavior of rigid bodies, and specifically of rectangular blocks, has been extensively documented [e.g., 2,3]. Moreover, the rocking and impact behavior using finite elements (FE) software has been assessed by the development of contact elements, allowing the simulation of sliding between bodies, non-linear effects at the contact interfaces and a better control over damping in the model [4]. However, dealing with contact problems in FE software is still cumbersome. Because of this fact, the results presented next are derived from a physical model implemented in MATLAB[®] that enables full control of the contact forces and the system dynamic parameters.

This article presents the 2D analytical formulation of the problem, while the contact parameters have been calibrated through experimental analysis of barrels and racks samples. Also, a validation of the model using experimental results from previous research is presented [1]. The current formulation includes special features such as the dynamic interaction between the ground, barrels, and racks, using contact elements, large displacements, local energy dissipation, upthrow, and rocking and sliding behavior in 2D. The model presented

is a good complement of the available experimental data, which enables the designer to extrapolate results to other wine barrel stacks configurations.

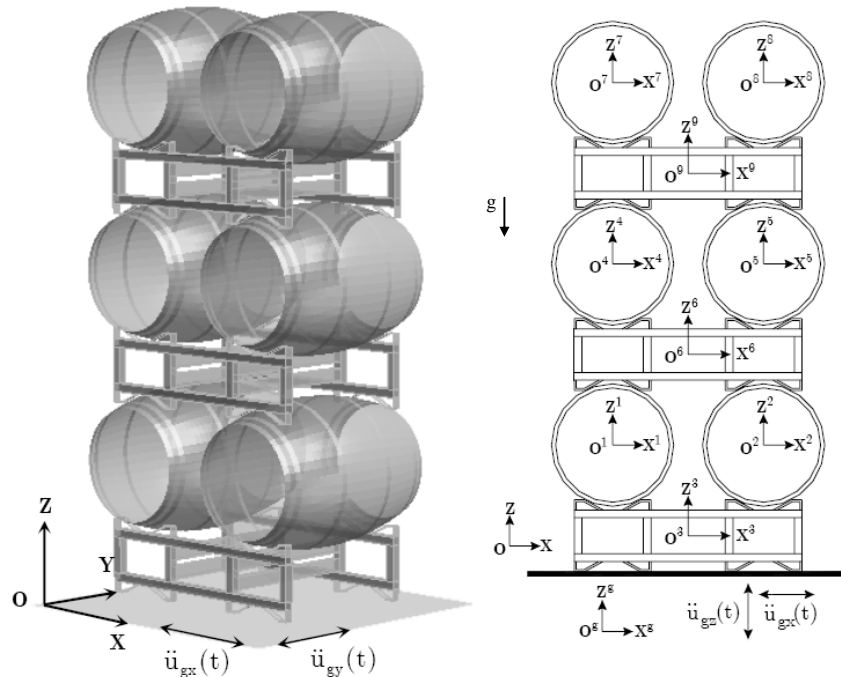


Figure 1 Typical (2,4) barrel configuration and 2D rack-barrel structural model considered

2. TWO-DIMENSIONAL STRUCTURAL MODEL

A generic view of the structural model considered is shown in Figure 1. Because of length limitations, this article deals exclusively with the 2D-model of the system and a complete description of the 3D-model and behavior is provided elsewhere [5]. The analysis framework follows the fundamental steps of structural analysis: (i) kinematics, where the position, velocity and acceleration of a point on the rigid body are described in terms of generalized coordinates; (ii) action-deformation, where the relationships between forces and deformations of the contact elements are established; and (iii) equilibrium, stated through the principle of virtual displacements.

Let us consider the typical (2,4) rack-barrel configuration presented in Figure 1. In this model each body has its own local frame of reference that is fixed to the body, denoted $\Gamma^i\{X^i, Y^i, Z^i\}$. There is also a global reference frame denoted as $\Gamma\{X, Y, Z\}$. The base of the structure is also considered as a rigid body with its own local reference frame $\Gamma^g\{X^g, Y^g, Z^g\}$. Please note that the horizontal and vertical components of the base displacement $\mathbf{u}_g = [\mathbf{u}_{gx} \ \mathbf{u}_{gz}]$ and base velocity $\dot{\mathbf{u}}_g = [\dot{\mathbf{u}}_{gx} \ \dot{\mathbf{u}}_{gz}]$ are known, which correspond to the seismic input displacement and velocity. Shown in Figure 2 are the typical dimensions of barrel and racks, as well as the geometry and axes considered in the analysis. Each barrel is simply supported on the top of the indicated cradles. Therefore barrels may slide, rotate, be in contact or ejected from those cradles during an earthquake.

The unconstrained motion of a rigid body in the plane is described using three independent generalized coordinates $\mathbf{q}^i = [\mathbf{R}^{iT} \ \theta^i]^T$, where $\mathbf{R}^i = [\mathbf{R}_x^i \ \mathbf{R}_z^i]^T$ defines the position of the origin O^i of the local reference frame $X^i Z^i$ with respect to the inertial reference frame XZ , and the coordinate θ^i defines its orientation relative to a horizontal axis (Figure 3a). Therefore if u^i are the local coordinates of an arbitrary point \mathbf{P} on the rigid body, the absolute position, velocity and acceleration of the point are

$$\begin{aligned} \mathbf{r}^i &= \mathbf{R}^i + \mathbf{A}^i \bar{\mathbf{u}}^i = \begin{bmatrix} \mathbf{I} & \mathbf{0} \end{bmatrix} \mathbf{q}^i + \mathbf{A}^i \bar{\mathbf{u}}^i \\ \dot{\mathbf{r}}^i &= \dot{\mathbf{R}}^i + \dot{\mathbf{A}}^i \bar{\mathbf{u}}^i = \begin{bmatrix} \mathbf{I} & \mathbf{H}^i \bar{\mathbf{u}}^i \end{bmatrix} \dot{\mathbf{q}}^i \\ \ddot{\mathbf{r}}^i &= \ddot{\mathbf{R}}^i + \ddot{\mathbf{A}}^i \bar{\mathbf{u}}^i = \begin{bmatrix} \mathbf{I} & \mathbf{H}^i \bar{\mathbf{u}}^i \end{bmatrix} \ddot{\mathbf{q}}^i - \mathbf{A}^i \bar{\mathbf{u}}^i (\omega^i)^2 \end{aligned} \quad (2.1)$$

where $\omega^i = \dot{\theta}^i$ is the angular velocity of the i -th body and the matrices \mathbf{A}^i and \mathbf{H}^i are given by

$$\mathbf{A}^i = \begin{bmatrix} \cos \theta^i & -\sin \theta^i \\ \sin \theta^i & \cos \theta^i \end{bmatrix} \quad \text{and} \quad \mathbf{H}^i = \frac{d}{d\theta^i} \mathbf{A}^i \quad (2.2)$$

and satisfy $\mathbf{A}^{iT} \mathbf{A}^i = \mathbf{I}_{2 \times 2}$, i.e., \mathbf{A}^i is an orthonormal matrix.

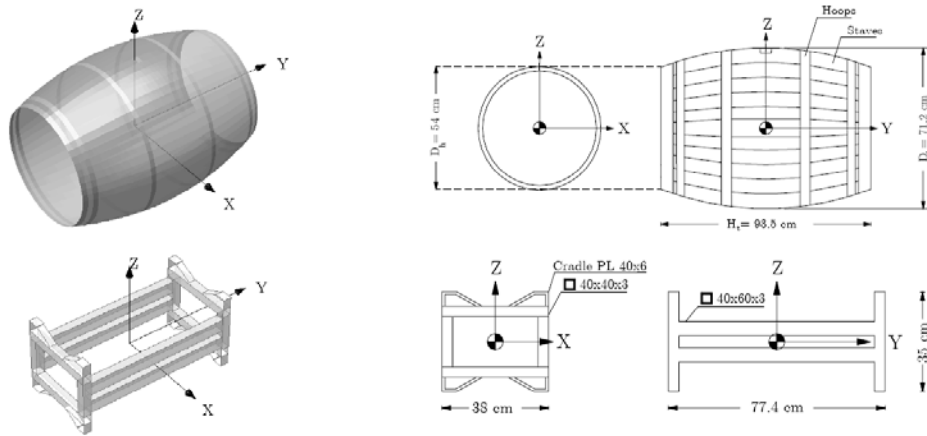


Figure 2 Typical dimensions of barrel and cradle considered in the study

The boundary of the i -th body is defined by a function $\Phi^i=0$ (Figure 3b), such that all points in the interior satisfy the relation $\Phi^i(\bar{\mathbf{u}}^i)=0$. The simplest case would be the circular function of a section of a barrel with diameter D_h (Figure 2), i.e.,

$$\Phi^i(\bar{\mathbf{u}}^i) = \bar{\mathbf{u}}^{iT} \bar{\mathbf{u}}^i - \frac{1}{4} D_h^2 \quad (2.3)$$

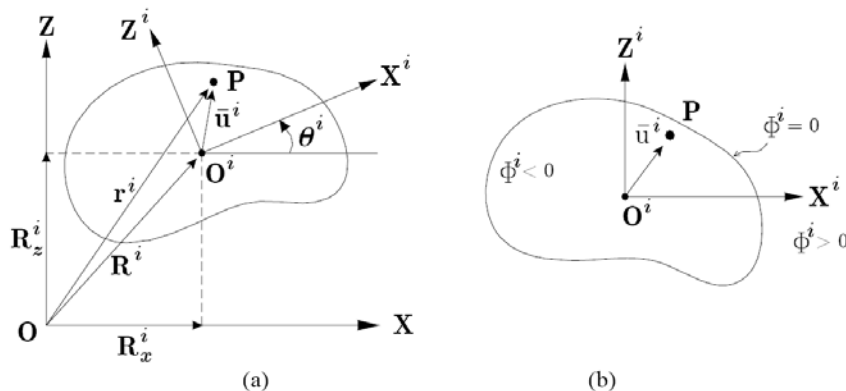


Figure 3 Definition of degrees of freedom and boundaries

To define the contact condition between two bodies, denote i as the target body and j as the contact body. The boundary of the contact body $\Phi^j=0$ is discretized on nodes u^j as depicted in Figure 4. Thus, two bodies are in contact at point Q if exists a node \bar{u}^j_Q of the j -th contact surface that is inside the i -th target body. Hence, the condition $\Phi^i(\bar{u}^j_Q) < 0$ must hold, where \bar{u}^j_Q are the coordinates of node Q relative to the reference frame of the i -th target body. Because of the orthonormality of the transformation matrix \mathbf{A}^i , the vector \bar{u}^j_Q is given by $\bar{u}^j_Q = \mathbf{A}^{iT}(\mathbf{r}'_Q - \mathbf{R}^i)$, where \mathbf{r}'_Q is also equal to $\mathbf{r}'_Q = \mathbf{R}^j + \mathbf{A}^j \bar{u}^j_Q$.

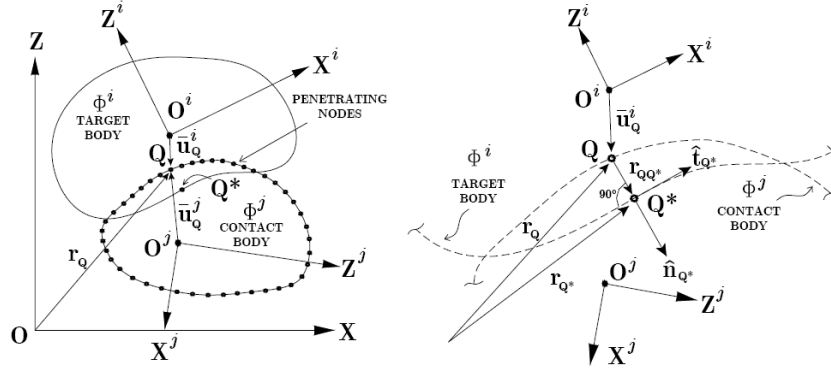


Figure 4 Definition of contact elements and penetration of surfaces

The penetrating node Q of the j -th contact body is related to a companion node Q^* on the target surface such that $\Phi^i(\bar{u}^j_{Q^*})=0$, and the penetration vector $\mathbf{r}_{QQ^*} = \mathbf{r}_{Q^*} - \mathbf{r}_Q$ is normal to the target surface and determines the direction of the normal vector n at point Q^* (Figure 4). Thus,

$$\mathbf{r}_{QQ^*} = \lambda \mathbf{A}^i \nabla \Phi^i \Big|_{\bar{u} = \bar{u}^j_{Q^*}}, \quad \hat{\mathbf{n}} = \frac{\mathbf{r}_{QQ^*}}{|\mathbf{r}_{QQ^*}|} \quad (2.4)$$

In this equation, $\lambda \neq 0$ is real and $\nabla \Phi^i$ is the gradient to the surface Φ^i at point Q^* . The relative velocity $\dot{\mathbf{r}} = \dot{\mathbf{r}}_{Q^*} - \dot{\mathbf{r}}_Q$ between nodes Q and Q^* , can be projected into a velocity component \mathbf{v}^n and \mathbf{v}^t that are normal and tangential to the target surface, respectively

$$\begin{aligned} \mathbf{v}^n &= (\dot{\mathbf{r}}_{QQ^*} \cdot \hat{\mathbf{n}}) \hat{\mathbf{n}} = v^n \hat{\mathbf{n}} \\ \mathbf{v}^t &= \dot{\mathbf{r}}_{QQ^*} - \mathbf{v}^n = v^t \hat{\mathbf{t}} \end{aligned} \quad (2.5)$$

where $\hat{\mathbf{t}} = \mathbf{v}^t / |\mathbf{v}^t|$ is the unit vector tangent to the boundary of the target body at point Q^* . The contact force \mathbf{F}_{QQ^*} associated with nodes Q and Q^* is developed by a contact element capable of transmitting forces that are normal and tangential to the boundary of the target body along the orthogonal directions n and t , respectively. Then, $\mathbf{F}_{QQ^*} = f^n \hat{\mathbf{n}} + f^t \hat{\mathbf{t}}$, where the magnitude of the normal component f^n was modeled using a linear spring element in parallel with a speed-gap damper element, which allows a dissipative penetration of the surface but a perfectly elastic rebound (Figure 4). The constitutive relationship of the normal contact force is

$$f^n = \begin{cases} \bar{k} |\mathbf{r}_{QQ^*}| + \bar{c} v^n & \text{if } v^n > 0 \\ \bar{k} |\mathbf{r}_{QQ^*}| & \text{if } v^n \leq 0 \end{cases} \quad (2.6)$$

where \bar{k} and \bar{c} are stiffness and damping contact parameters that need to be calibrated experimentally. On the other hand, the magnitude of the tangential component f^t was modeled using Coulomb's dry friction theory, i.e., $f^t = \mu f^n$, where μ is the sliding coefficient of friction at the contact interfaces.

Consequently, the resultants forces conjugated with the generalized coordinates \mathbf{q}^i and \mathbf{q}^j are computed by adding the force contributions of all contact elements. The best way to do so is to apply the principle of virtual displacements, leading to the generalized forces

$$\mathbf{F}^{ij} = \sum_Q \left(\frac{\partial \mathbf{r}_{Q^*}^i}{\partial \mathbf{q}^i} \right)^T \mathbf{F}_{Q^*} = \sum_Q [\mathbf{I} \quad \mathbf{H}^i \bar{\mathbf{u}}_{Q^*}^i]^T \mathbf{F}_{Q^*}$$

$$\mathbf{F}^{ji} = -\sum_Q \left(\frac{\partial \mathbf{r}_{Q^*}^j}{\partial \mathbf{q}^j} \right)^T \mathbf{F}_{Q^*} = -\sum_Q [\mathbf{I} \quad \mathbf{H}^j \bar{\mathbf{u}}_{Q^*}^j]^T \mathbf{F}_{Q^*}$$
(2.7)

In general, the accuracy in the computation of the contact forces using this procedure depends on the spatial discretization used for the contact surface and the smoothness characteristics of the target surfaces. In order to state the equilibrium of the i -th body, the work done by internal forces is equal to the work done by external forces, hence $\mathbf{W}_I^i + \mathbf{W}_C^i = \mathbf{W}_E^i$. Substituting these results, the dynamic equation of motion for the i -th body is

$$\mathbf{M}^i \ddot{\mathbf{q}}^i - \mathbf{C}_v^i \dot{\mathbf{q}}^i + \mathbf{F}^{ij} = \mathbf{P}^i$$
(2.8)

where \mathbf{M}^i and \mathbf{C}_v^i represent the mass and viscous damping matrices of the i -th body, respectively, and \mathbf{P}^i , the external forces on this body. Assembling similar equations for each of the bodies of the system, the global equations of motion for N interacting bodies are

$$\mathbf{M}^i \ddot{\mathbf{q}}^i - \mathbf{C}_v^i \dot{\mathbf{q}}^i + \mathbf{F}^i = \mathbf{P}^i \quad \text{where} \quad \mathbf{F}^i = \sum_{k \neq i} \mathbf{F}^{ik}$$
(2.9)

3. NUMERICAL EXAMPLE

A numerical example based on the preceding formulation is presented next. The barrel-stack configuration considered is commonly used in local wineries and consists of 6 barrels arranged as shown in Figure 5 and racks type 2. The pairs of contact and target bodies are indicated in Figure 5b, where the arrow starts in a contact body and ends at the corresponding target body.

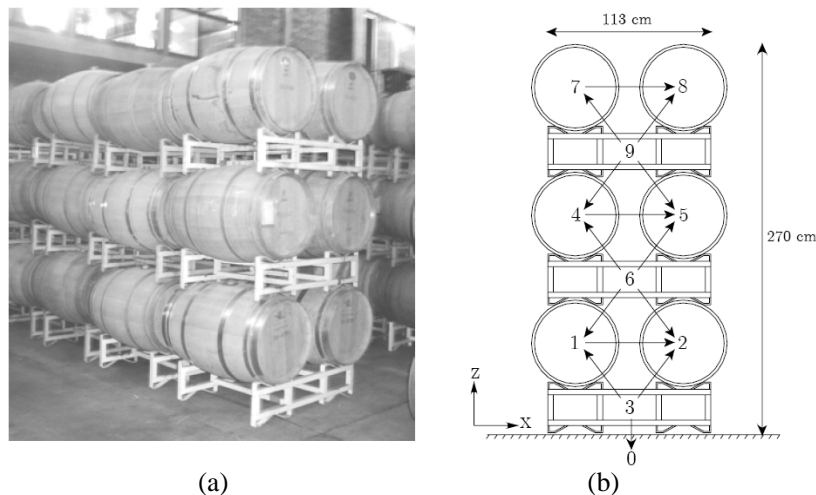


Figure 5 (a) Typical (3,2) barrel rack configuration at Veramonte Winery (Chile), and (b) pairs of contact and target bodies

The ground motion used in this example is the N-S component of the LA-Hollywood Storage record (Northridge, 1994) scaled to a PGV=60cm/s. The constants of the contact element \bar{k} , \bar{c} , μ_{rg} , μ_{br} were calibrated experimentally as shown elsewhere [5] with μ_{rg} and μ_{br} are the rack-ground and rack-barrel friction coefficients. Two values for the former were considered in this example $\mu_{rg} = 0.4$ and 0.1. The barrel stack

sustains 10s of ground motion prior to collapsing by rocking of the 2 upper levels (Figure 6a). It is apparent from the horizontal displacement history (upper plot of Figure 6c) that a collapse mechanism begins right after the pick ground velocity. Due to the high friction coefficient $\mu_{rg} = 0.4$, the residual displacement between the lower rack and the ground was only 2cm.

Shown in Figure 6b are the normal contact stresses of barrel 1, where the shadowed area represents the stress distribution computed from static analysis, and the thick line is the stress envelope due to the dynamic effects. It is apparent that the average stress amplification as a result of the impact between bodies was about 2.9 times. Also, notice that the dynamic stress envelope covers a larger portion of the top surface of barrel 1 as a result of the sliding of the racks along this surface. The opposite occurs at the bottom surface of barrel 1, where the initial static distribution is only amplified by dynamic effects without sliding.

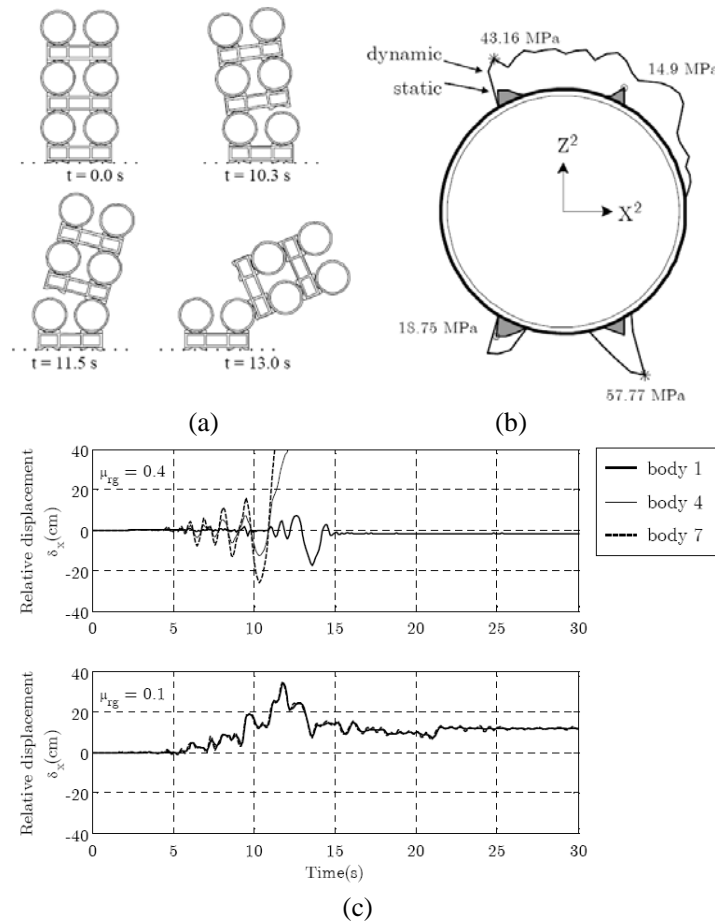


Figure 6 Earthquake response of the example model (a) stack rocking collapse sequence, (b) static and dynamic envelope of normal contact stress on body 2, and (c) relative horizontal displacement history of bodies 1, 4 and 7 for a rack-to ground friction of $\mu_{rg} = 0.4$ and $\mu_{rg} = 0.1$.

Finally, the lower plot of Figure 6c shows the horizontal displacement history of barrels 1, 4, and 7 for a friction coefficient of $\mu_{rg} = 0.1$. This lower friction coefficient causes the rack to slide horizontally as a rigid body preventing the rocking behavior. This isolation leads to a larger residual displacement, but prevents the collapse of the barrel-rack configuration.

3. COMPARISON WITH EXPERIMENTAL MODEL

Let us consider the experimental behavior [1] of a half-scale rack-barrel stack of 4 levels (Figure 7). The barrel

stack was subjected first to a sinusoidal ground motion with amplitude of 2in and a period of 0.76s. After 2s of the input motion, the barrels of the fourth level and the respective rack were ejected to each side of the stack [1]. In the analytical model, pairs of contact and target bodies were selected as in Figure 7a. The contact element parameters \bar{k} and \bar{c} in this case were calibrated in order to obtain the same overall response as for the experimental model, leading to $\bar{k}=9.8$ kN/cm and $\bar{c}=22.0$ Ns/cm. These values are 10% and 16% greater than the parameters determined experimentally for local barrels and racks. The friction coefficients selected were $\mu_{br}=0.22$ and $\mu_{rg}=0.5$.

The ground motion input was scaled down in order to maintain the acceleration constant, leading to an amplitude of 4in and a period of $0.76\sqrt{2}$ s. The observed mode of collapse for the real scale analytical model was identical as that of the experimental model, i.e., the top barrel ejection [1]. It can be shown that the first barrel to fall, body 11, was ejected at $t=1.5s$ and the second barrel, body 10, at $t=2.5s$. Please notice that the aspect ratio of this barrel-rack configuration leads to a very flexible system capable of developing large relative displacements among elements. For instance, the maximum relative displacement of the top barrel with respect to the base is 5.2% of the stack height.

A schematic comparison of the collapse sequence for the experimental and analytical models is presented in Figure 7b, where the displaced configuration is given at equivalent instants: t^* for the experimental model and $t=\sqrt{2}t^*$ for the analytical (real size) model. The similarity on the overall earthquake behavior of the barrel stack is apparent. It also enable us to confirm the usefulness of the formulation and the calibration of the parameters \bar{k} , \bar{c} and μ_{br} . It is interesting to note that not only the same collapse mode was predicted, but also the analytical model proved to be robust against variations of the contact element parameters within 10%. Based on this analytical model, several interesting results can be analyzed for this rack-barrel system. For instance, the normal stress envelopes were drafted on the surface of the barrel and racks resulting from static and dynamic analysis (Figure 7c). It is apparent that the normal stresses due to the dynamic interaction between bodies increased 3.0 times the stresses due to self weight.

The same configuration was analyzed along the longitudinal direction using the longitudinal cross-section of a barrel and a rack type 1, which is not shown for the sake of brevity. For every contact body, the corresponding target bodies are located above and below. Subjected to the same sinusoidal input as previously, the rack-barrel stack endured 4.5s of ground motion before becoming unstable. The mechanism was such that the rack from the second level (body 4) slid progressively on the barrel below, until the cradle reached the edge of the barrel causing the upper bodies to overturn. This mode of collapse, denoted earlier as "rack sliding", is one of the most common mechanisms in shaking table experiments done on longitudinal specimens [1].

4. CONCLUSIONS

In this investigation a structure-based physical model was developed to represent the earthquake behavior of wine barrel stacks, assuming that all bodies are rigid and that their interaction forces are properly represented by the use of contact elements. By using this analytical model, it is possible to reproduce the overall earthquake behavior and the likely modes of collapse of these systems when adequate contact element parameters are used. This model sets the basis for carrying out larger parametric studies with different barrel-rack configurations and ground motions. This is relevant because these systems are very sensitive to different ground motion and local site characteristics and experimental results may not account for all different practical situations. The contact elements developed enable us to monitor the forces that are developed at the rack-ground and rack-barrel interfaces, and hence to improve their contact design as well as evaluate their eventual failure. In particular, it was found that the maximum normal stresses on a body when the barrel stack is subjected to a prescribed ground motion may be as large as 3 times the maximum stresses due to self-weight. Moreover, analytical results on the benchmark experimental case considered were able to predict the collapse modes observed in the transverse as well as longitudinal directions of the rack-barrel stack.

5. ACKNOWLEDGEMENTS

This research has been sponsored by the Chilean National Fund for Science and Technology, Fondecyt, under Grant # 1040331. The authors are grateful for this support.

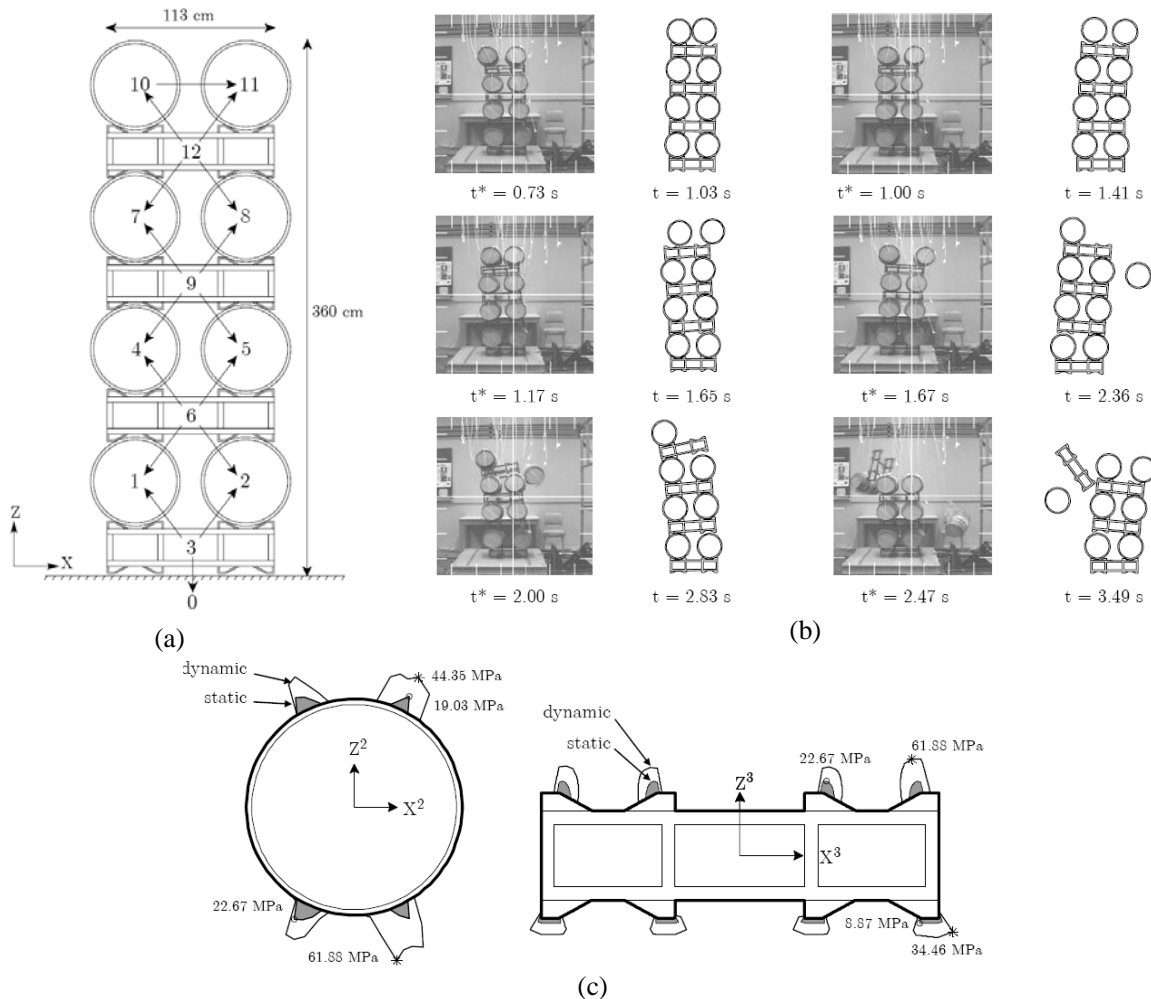


Figure 7 Comparison of the experimental and analytical behavior for the (2,4) barrel-rack configuration: (a) collapse sequence for transverse analysis, and (b) normal stress envelopes on bodies 2 and 3 resulting from static and dynamic analysis. (Experimental results extracted for comparison from reference [2]).

REFERENCES

1. Marrow J. & Makris N. (2000) Experimental studies on the earthquake performance of wine barrel stacks. University of California, Berkeley, USA.
2. Housner, G.W. (1963) The behavior of Inverted Pendulum during Earthquakes. Bulletin of the Seismological Society of America, 3 (2), pp. 403 - 417.
3. Makris, N. & Roussos, Y. (1998) Rocking Response and Overturning of Equipment under Horizontal Pulse-Type Motions. University of California Berkeley.
4. Lennon R. Earthquake Rocking Behavior in Finite Element Models, 2004
5. Candia G., de la Llera J.C., Almazán J.L. (2008). A physical model for dynamic analysis of wine barrel stacks. Submitted for publication to Engineering Structures.